Nitroreductase sensitive styryl-benzothiazole profluorescent probes for the visualization of mitochondria under normoxic conditions

Mauro Safir Filho, Pascal Dao, Anthony Martin, Rachid Benhida

Nitroreductase sensitive styryl-benzothiazole profluorescent probes for the visualization of mitochondria under normoxic conditions.

Mauro Safir Filho,[a] Pascal Dao,[a] Anthony R. Martin,[a,*] and Rachid Benhida,[a,b,*]

[a] *Université Côte d'Azur, CNRS, Institut de Chimie de Nice UMR7272, Nice, France*
[b] *Mohamed VI Polytechnic University, UM6P, 43150, Ben Guerir, Morocco*

Abstract

Selective imaging of cellular organelles is a rapidly expanding field of research. Within this context we describe the development of two novel profluorescent probes, **MitoP-2** and **MitoP-3**, for the precise staining of mitochondrial compartments. Herein, we demonstrate that caged, non-fluorescent styryl-benzothiazole probes harbouring a *p*-nitrobenzyl motif can be converted into their parent fluorophore under the action of the nitroreductase (NTR) enzyme. Two probes, **MitoP-2** and **MitoP-3**, exhibited a turn-ON fluorescence signalling in NTR enzymatic assays. In addition, they also proved successful in the staining of the mitochondria in cellular experiments under normoxic conditions. Interestingly, while **MitoP-2** and **MitoP-3** structures only differ by the presence of a cationic mitochondrial-targeting unit, both were equally efficient in the staining of mitochondria. Hence, an activity-based approach (**MitoP-2**) is sufficient for the precise targeting of mitochondria and the use of cationic mitochondria-targeting units (phosphonium present on **MitoP-3**) can be considered superfluous in this case.

Keywords
Nitroreductase, mitochondria staining, fluorescence imaging, normoxic conditions, turn-ON fluorescence sensing, styryl-benzothiazole fluorophores.

1. Introduction

Selective imaging of cellular organelles such as nucleus, lysosomes, Golgi apparatus, endoplasmic reticulum or mitochondria is an expanding field of research.[1] The visualization and characterization of biological processes using selective imaging have rapidly gained importance in many aspects of biomedical research, including drug discovery. In fact, the emergence of novel and more powerful optical technologies and the availability of large variety of molecular probes and sensors, fostered remarkable progresses during the last decades.[2] The rapid growth in the number of available fluorescent systems offers a versatile toolbox to study a wide diversity of cellular processes.[3,4] Therefore, fluorescence-based methods have recently become one of the most used approaches to image living organisms, providing a rapid, selective, sensitive and non-invasive way to monitor and uncover biological processes.[2]

Mitochondria are unique organelles that play a central role in energy production and regulation of cellular metabolism. Denoted as the "powerhouse", the mitochondrial machinery generates most of the ATP required to ensure homeostasis, cell survival, and to deliver biosynthetic intermediates/metabolites that sustain cell proliferation under regular nutrition conditions.[5] Nonetheless, recent evidences further demonstrate that mitochondria organelles also integrate a complex and dynamic network within the cytosol; it regulates many cell signalling pathways and cellular stress responses that extend even beyond the cell boundaries, including autophagy, apoptosis and angiogenesis.[6–8] Thereby, it is not surprising that mitochondrial dysfunctions can bolster the development of various human diseases, including cancers.[5] In this context, mitochondrial imaging has become an important tool in the investigation of mitochondrial stress and in the development of drugs targeting this organelle.[9]

Heretofore, numerous probes have been reported to visualize mitochondria.[10] These probes encompass cationic dyes such as cyanines, BODIPYs and rhodamines, and fluorophores tethered to lipophilic cations.[11] Due to their positive charge, these molecules can accumulate into the mitochondrial compartments because of the negative polarization of the mitochondrial membrane.[12] Recently, evidences of mitochondrial nitroreductase (NTR) activity present in human cells under normoxic conditions have prompted the development of more sophisticated strategies resorting to the NTRs activation of inactive profluorophores. Such approaches could improve the mitochondria staining accuracy.[9,13,14] NTRs are enzymes that catalyse the reduction of nitroaromatic substrates into their corresponding (hydroxy)anilines using either NADH or NADPH as the cofactor. NTRs are divided into two categories: the oxygen insensitive Type I NTRs, which was found to be expressed within the mitochondria of cancerous and healthy cells[9,13] and the oxygen dependent Type II NTRs, overexpressed in solid tumours and widely accepted as a marker of hypoxia.[15,16] Many fluorescent probes have already been reported to monitor and visualize NTRs activities *in cellulo* and *in vivo*.[17,18] Nevertheless, most of these probes are reported for type II NTRs and used under hypoxic conditions. In contrast, scarce examples of profluorescent probes devoted to the visualization of mitochondrial NTRs activities under normoxic conditions have been described to date (Figure 1).[9,13,19]

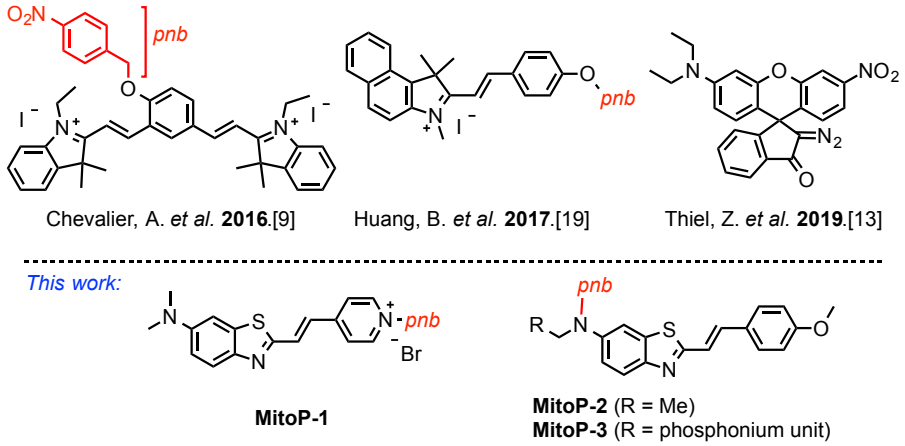

Figure 1. Profluorescent probes reported for the visualization of mitochondrial NTR activity under normoxic conditions, and the probes described in this work.

2. Experimental

2.1. General considerations

All chemical reagents and solvents were obtained from commercial sources (Aldrich, Acros, Alfa Aesar) and were used as supplied. All NMR spectra (^{1}H, ^{13}C and ^{31}P) were recorded on 400 MHz Bruker Advance Spectrometer with samples dissolved in $CDCl_3$, CD_2Cl_2 or DMSO-d_6. Solvent residual signals were used as internal references: 7.26 ppm for $CDCl_3$, 5.32 ppm for CD_2Cl_2 and 2.50 ppm for DMSO-d_6 for ^{1}H NMR experiments, and 77.16 ppm for $CDCl_3$, 53.84 ppm for CD_2Cl_2 and 39.52 ppm for DMSO-d_6 for ^{13}C NMR experiments. Chemical shifts (δ) are given in ppm to the nearest 0.01 (^{1}H), 0.1 ppm (^{13}C) or 0.1 ppm (^{31}P). ^{13}C and ^{31}P NMRs are proton decoupled. The coupling constants (*J*) are given in Hertz (Hz). The signals are reported as follows: chemical shift, multiplicity (s = singlet, d = doublet, t = triplet, m = multiplet, dd = doublet of doublets, br = broad), coupling constants (*J*) and integration. High Resolution Mass Spectra (HRMS) were recorded on a ThermoFisher Q Exactive (ESI-MS) at a resolution of 65000 at m/z 200. UV-vis absorption spectra were recorded on V-750 spectrophotometer (Jasco) using probe concentration of *ca.* 10^{-5} M. Fluorescence emission spectra were recorded on FluoroMax 4.0 spectrofluorometer (Jobin Yvon, Horiba) using probe concentration *ca.* 10^{-6} M. Quinine sulphate (ϕ_{fl} = 54 % in 0.1 M H_2SO_4) was used as the standard reference for the quantum yield measurements.

2.2. Synthetic procedures

Synthesis of compound **1**: Compound **3a** (192 mg, 1.0 mmol), potassium *tert*-butoxide (112 mg, 1 mmol, 1 equiv.), and 4-pyridinecarboxaldehyde (214 mg, 2.0 mmol, 2 equiv.) were dissolved in 10 mL DMSO and stirred for 2 hours at room temperature. After complete conversion of the starting material, the crude was diluted with 100 mL of water and extracted with ethyl acetate (3 × 30 mL). The organic phase was combined, dried over magnesium sulphate, and the solvent was removed under reduced pressure. The crude was purified by flash column chromatography on silica gel using cyclohexane-ethyl acetate mixtures as the eluent (100-0 to 60-40) to afford fluorophore **1**. Further recrystallized from methanol afford 177 mg (63 % yield) of **1** as an orange solid. ^{1}H NMR (400 MHz, $CDCl_3$) δ 8.62 (dd, *J* = 4.6, 1.5 Hz, 2H), 7.84 (d, *J* = 9.1 Hz, 1H), 7.53 (d, *J* = 16.2 Hz, 1H), 7.38 (dd, *J* = 4.8, 1.3 Hz, 2H), 7.24 (d, *J* = 15.8 Hz, 1H), 7.06 (d, *J* = 2.5 Hz, 1H), 6.95 (dd, *J* = 9.1, 2.5 Hz, 1H), 3.06 (s, 6H). ^{13}C NMR (101 MHz, $CDCl_3$) δ 160.6, 150.6, 149.4, 145.8, 143.3, 137.3, 132.1, 126.9, 123.7, 121.2, 113.7, 102.6, 41.0. HRMS (ESI) *m/z*: $[M+H]^+$ Calcd for $C_{16}H_{16}N_3S$ 282.1059; Found 282.1057.

Synthesis of **MitoP-1**: Compound **1** (50 mg, 0.18 mmol), and *p*-nitrobenzylbromide (42 mg, 0.2 mmol, 1.1 equiv.) were suspended in 5 mL of toluene and heated under reflux until complete consumption of the starting material (TLC). Then, the solvent was removed under reduced pressure

and the crude was purified by flash column chromatography on silica gel using dichloromethane-methanol mixtures as the eluent (100-0 to 90-10). The desired probe **MitoP-1** was obtained as a non-fluorescent dark solid. Yield: 32% (29 mg). ^{1}H NMR (400 MHz, DMSO-*d6*) δ 9.14 (d, *J* = 6.7 Hz, 2H), 8.45 (d, *J* = 6.7 Hz, 2H), 8.30 (d, *J* = 8.7 Hz, 2H), 8.25 (d, *J* = 16.1 Hz, 1H), 7.86 (d, *J* = 9.1 Hz, 1H), 7.78 (d, *J* = 8.7 Hz, 2H), 7.65 (d, *J* = 16.1 Hz, 1H), 7.34 (d, *J* = 2.4 Hz, 1H), 7.07 (dd, *J* = 9.2, 2.5 Hz, 1H), 5.94 (s, 2H), 3.04 (s, 6H). ^{13}C NMR (101 MHz, DMSO-*d6*) δ 157.9, 152.2, 149.6, 147.9, 145.2, 144.8, 141.4, 137.9, 133.7, 129.9, 127.9, 124.9, 124.1, 123.8, 114.1, 102.4, 61.4, 40.3. HRMS (ESI) *m/z*: $[M+H]^+$ Calcd for $C_{23}H_{21}O_2N_4S$ 417.1380; Found 417.1375.

Synthesis of **MitoP-2**: Compound **2**[20] (50 mg, 0.16 mmol), potassium carbonate (44 mg, 0.32 mmol, 2 equiv.), *p*-nitrobenzylbromide (100 mg, 0.48 mmol, 3 equiv.), and potassium iodide (27 mg, 0.16 mmol, 1.0 equiv.) were suspended in 5 mL of acetonitrile and heated under reflux until complete consumption of the starting material (TLC). Next, the solvent was removed under reduced pressure and the crude was purified by flash column chromatography on silica gel using cyclohexane-ethyl acetate mixtures as the eluent (100-0 to 70-30). The desired probe **MitoP-2** was obtained as a non-fluorescent dark yellow solid. Yield: 58% (41 mg). ^{1}H NMR (400 MHz, $CDCl_3$) δ 8.19 (d, *J* = 8.8 Hz, 2H), 7.76 (d, *J* = 9.0 Hz, 1H), 7.49 (d, *J* = 8.7 Hz, 2H), 7.43 (d, *J* = 8.8 Hz, 2H), 7.30 (d, *J* = 16.2 Hz, 1H), 7.21 (d, *J* = 16.2 Hz, 1H), 6.99 (d, *J* = 2.5 Hz, 1H), 6.92 (d, *J* = 8.8 Hz, 2H), 6.82 (dd, *J* = 9.0, 2.6 Hz, 1H), 4.67 (s, 2H), 3.84 (s, 3H), 3.57 (q, *J* = 7.1 Hz, 2H), 1.29 (t, *J* = 7.1 Hz, 3H). ^{13}C NMR (101 MHz, $CDCl_3$) δ 163.3, 160.5, 147.4, 146.9, 146.3, 146.2, 136.8, 135.7, 128.7, 128.6, 127.4, 124.2, 123.3, 120.4, 114.5, 113.2, 103.2, 55.5, 54.4, 46.4, 12.4. HRMS (ESI) *m/z*: $[M+H]^+$ Calcd for $C_{25}H_{24}O_3N_3S$ 446.1533; Found 446.1527.

Synthesis of **MitoP-3**: (i) Compound **4** (160 mg, 0.56 mmol), potassium carbonate (154 mg, 1.12 mmol, 2 equiv.) and 1,6-diiodohexane (281 µL, 1.68 mmol, 3 equiv.) were suspended in 5 mL of acetonitrile and heated under reflux for 3 hours. Next, the solvent was removed under reduced pressure and the crude was purified by flash column chromatography on silica gel using cyclohexane-ethyl acetate mixtures as the eluent (100-0 to 90-10). The structure of the intermediate **4'** was confirmed by ^{1}H NMR and directly used for the next step. Yield: 61% (168 mg).

(ii) Intermediate **4'** (168 mg, 0.34 mmol), potassium carbonate (94 mg, 0.68 mmol, 2 equiv.), 4-nitrobenzylbromide (219 mg, 1.02 mmol, 3 equiv.) and potassium iodide (56 mg, 0.34 mmol, 1 equiv.) were suspended in 5 mL of acetonitrile and heated under reflux until complete consumption of the starting material (TLC). Next, the solvent was removed under reduced pressure and the crude was purified by flash column chromatography on silica gel using cyclohexane-ethyl acetate mixtures as the eluent (100-0 to 70-30). The intermediate **4''** was obtained as a non-fluorescent yellow oil. Yield: 49% (104 mg).

(iii) Intermediate **4''** (50 mg, 0.08 mmol) and triphenylphosphine (200 mg, 0.80 mmol, 10 equiv.) were dissolved in 10 mL of toluene and heated under reflux overnight. Then, the solvent was removed, and the crude was purified by flash column chromatography on silica gel using

dichloromethane-methanol mixtures as the eluent (100-0 to 95-5) to afford the desired **MitoP-3** probe in 28 % yield as a dark yellow solid (20 mg). ^{1}H NMR (400 MHz, CD_2Cl_2) δ 8.14 (d, *J* = 8.7 Hz, 2H), 7.85 – 7.81 (m, 3H), 7.78 – 7.66 (m, 13H), 7.50 (d, *J* = 8.8 Hz, 2H), 7.43 (d, *J* = 8.7 Hz, 2H), 7.29 (d, *J* = 16.2 Hz, 1H), 7.19 (d, *J* = 16.2 Hz, 1H), 7.03 (d, *J* = 2.5 Hz, 1H), 6.92 (d, *J* = 8.8 Hz, 2H), 6.80 (dd, *J* = 9.1, 2.5 Hz, 1H), 4.73 (s, 2H), 3.83 (s, 3H), 3.54 – 3.50 (m, 4H), 1.73 – 1.68 (m, 6H), 1.47 – 1.42 (m, 2H). ^{31}P NMR (162 MHz, CD_2Cl_2) δ 23.9. ^{13}C NMR (101 MHz, CD_2Cl_2) δ 163.1, 160.9, 147.5, 147.4, 146.7, 146.4, 137.1, 135.6, 135.5 (d, *J* = 3.0 Hz), 134.1 (d, *J* = 10.0 Hz), 130.8 (d, *J* = 12.5 Hz), 128.9, 128.9, 127.8, 124.2, 123.3, 120.7, 118.5 (d, *J* = 86.1 Hz), 114.7, 113.4, 103.6, 55.7, 55.2, 52.5, 30.8, 30.6, 27.1 (d, *J* = 71.9 Hz), 23.4 (d, *J* = 50.3 Hz), 22.8 (d, *J* = 4.5 Hz). HRMS (ESI) *m/z*: $[M+H]^+$ Calcd for $C_{47}H_{45}O_3N_3PS$ 762.2914; Found 762.2906.

2.3. In vitro NTR activity detection.

Probes (**MitoP-1**, **MitoP-2** and **MitoP-3**, 2 μM) were suspended in PBS buffer solutions (pH = 7.4) and incubated at 37 °C (using water bath) in the absence or presence of 2.5 μg/mL of *E. coli* nitroreductase (obtained from Sigma Aldrich) and nicotinamide adenosine dinucleotide phosphate (NADPH, 0.5 mM) during 6 hours. Then, the samples were diluted with an equal volume of DMSO prior to analysis. Fluorescence emission spectra were recorded at 20°C using the following instrumental parameters: λ_{ex} = 405 nm, with slit widths of 5 nm (for both excitation and emission).

2.4. Cell experiments

Human melanoma A375 cells were obtained from American Type Culture Collection (ATCC, Manassas, VA, USA) and cultured in Dubelcco's Modifued Eagle's Medium (DMEM) containing 10% fetal bovine serum (FBS) and 5% penicillin/streptomycin at 37°C in a 5% CO_2 incubator.

2.5. Confocal fluorescence imaging

Cultured cell (A375, 5×10^4 cells/well) were seeded overnight onto coverslips placed into 6-well plate and incubated at 37°C in a 5% CO_2 incubator overnight. On the next day, cover slips were rinsed with PBS followed by incubation with desired probes (0.1 μM) and/or Mitotracker Deep Red (0.1 μM) at 37°C for 5, 15 or 30 min. Samples were washes with PBS and fixed with paraformaldehyde 4% before the coverslips were mounted onto a microscope slide with Fluoromount aqueous mounting medium (Sigma Aldrich) before fluorescence imaging.
Confocal fluorescent imaging was performed using a confocal microscope Nikon A1R scan head on a Nikon Eclipse Ti stand, using a Plan Apo 63X oil 1.4 NA objective. The excitation channel used was a LASER diode 405 nm or 633 nm and the emission signal was collected with an internal PMT detector equipped with a 500-570 or 660-740 nm filter set, and the transmission signal was collected on an external PMT. Fluorescence intensity quantification was done using Fiji.

3. Results and discussion

To ensure the visualization of mitochondrial NTRs activities under normoxic condition, we developed novel profluorescent turn-ON probes by resorting to a family of benzothiazole-based push-pull fluorophores that were previously studied by our group for other applications.[20–22] The probes were designed in analogy with the existing tools for the sensing of NTR activity[16] and tracking of mitochondrial compartments in cells. Hence, the first step of our work consisted in the preparation of styryl-benzothiazole based fluorophores functionalized with a *p*-nitrobenzyl moiety as the NTR substrate. This *p*-nitrobenzyl motif would serve two purposes: 1- it could act as a fluorescence suppressor (or quencher) of the fluorophore core through a photoinduced electron transfer (PET) mechanism; 2- the nitroaromatic function would operate as the NTR substrate. This strategy should yield molecular systems that display localized fluorescence within mitochondria organelles with turn-ON responses (Figure 2). Two approaches for the tethering of the *p*-nitrobenzyl unit to the fluorophore scaffold were investigated. The first one relied on the *N*-benzylation of the pyridine group and the formation of the cationic benzylpyridinium salt (**MitoP-1**). Since this species is cationic, it could intrinsically target the mitochondrion. The second approach relied on the *N*-benzylation of the ethylamino moiety located at the 6-position of the benzothiazole core (**MitoP-2** and **MitoP-3**).

These architectures should allow for the investigation of two important features: the selective accumulation of these probes within the mitochondrial compartment (cationic **MitoP-1** *vs* neutral **MitoP-2**) and the specific release of the active fluorophore upon mitochondrial NTR processing of the *p*-nitrobenzyl unit.

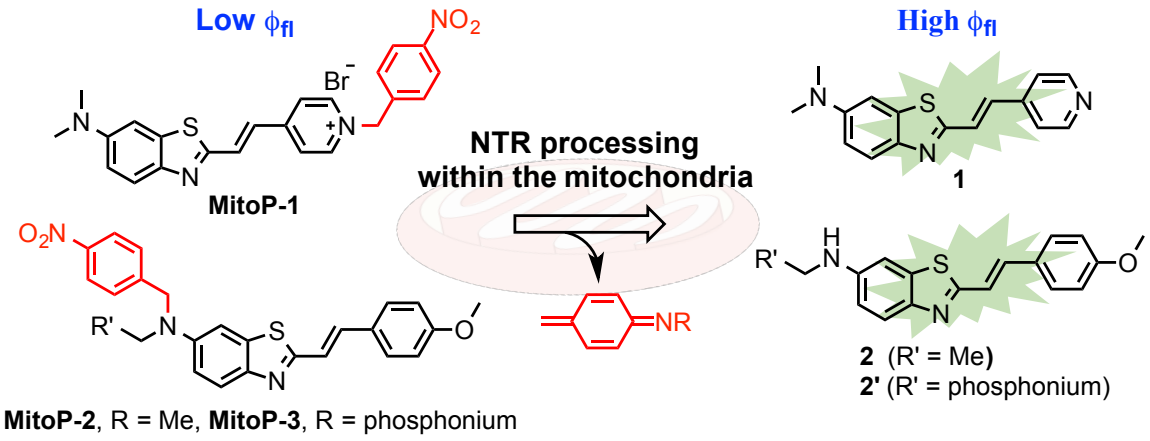

Figure 2. Proposed mode of activation of **MitoP-1**-**MitoP-3**, triggered by mitochondrial NTRs.

Synthesis

The preparation of **MitoP-1** and **MitoP-2** probes is straightforward. It is performed following a two-step sequence starting from the relevant 6-aklylamino-2-methylbenzothiazole (**3a** and **3b** for **MitoP-1** and **MitoP-2**, respectively - *Scheme 1*). Synthesis of **MitoP-1** commences with a Knoevenagel condensation between **3a** and the isonicotinaldehyde, using *t*BuOK as the base. The resulting fluorophore (**1**) is isolated in a 63% yield. Then, **1** is alkylated onto the nitrogen of the pyridine using an excess of *p*-nitrobenzyl bromide in refluxing toluene. The target pyridinium compound, **MitoP-1**, is obtained in a 32% yield after chromatographic purification on silica gel. Following this synthetic route, **MitoP-2** was prepared starting from the 6-ethylamino-2-methylbenzothiazole **3b** and *p*-anisaldehyde. The Knoevenagel condensation yielded **2**, as previously reported,[20] and the subsequent alkylation using *p*-nitrobenzyl bromide, potassium carbonate and potassium iodide, afforded the probe **MitoP-2** in decent yield (58% - *Scheme 1*).

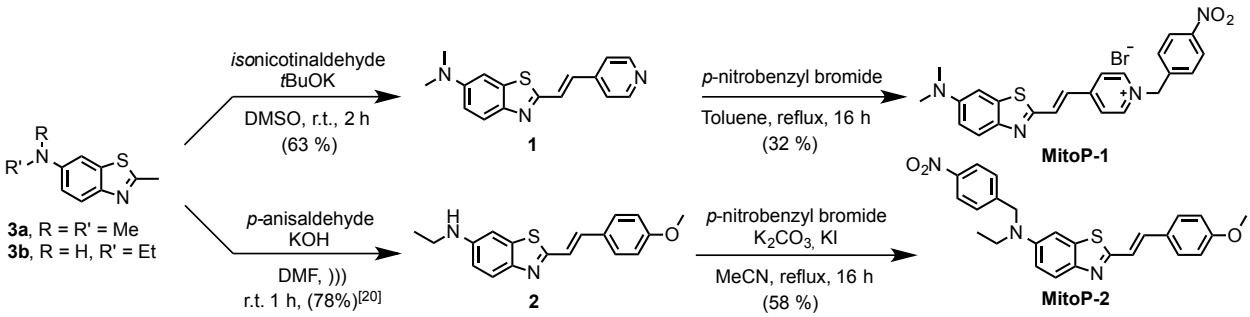

Scheme 1. Synthesis of probes **MitoP-1** and **MitoP-2**.

To complement our study, we prepared a third probe, **MitoP-3** (Figure 3), analogous to **MitoP-2**, harbouring a mitochondria-targeting triphenylphosphonium cation. This probe was specifically engineered to merge the spectroscopic properties of **MitoP-2** with the expected higher tendency of mitochondrial accumulation driven by the tethering of the cationic moiety.

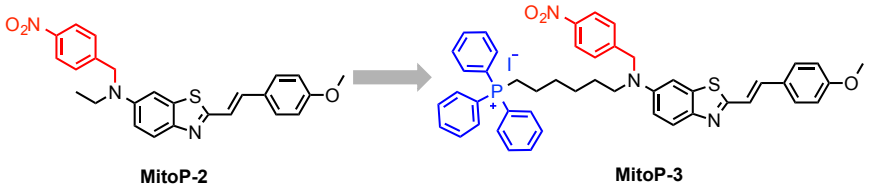

Figure 3. Chemical structure of **MitoP-2** and its analogue **MitoP-3** harbouring the cationic triphenylphosphonium as a mitochondria-targeting unit.

Probe **MitoP-3** was prepared in a one-pot three-step synthetic strategy, starting from compound **4** previously reported by our group (*Scheme 2*).[20] Firstly, **4** was *N*-alkylated using 1,6-diiodohexane to yield **4'** that bears a 6-iodohexyl moiety. Next, a second *N*-alkylation reaction using *p*-nitrobenzyl bromide furnished the key intermediate compound **4''**. Finally, the treatment

of **4''** with an excess of triphenylphosphine afforded the desired probe, **MitoP-3**, in 8% unoptimized overall yield (3 steps).

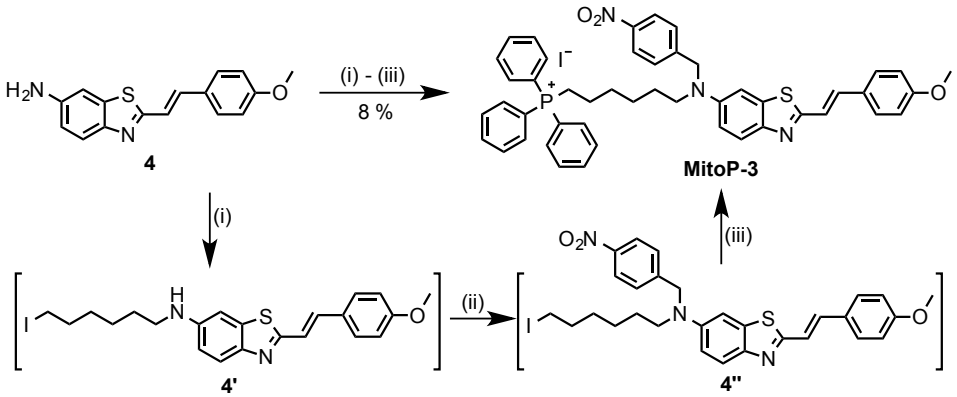

Scheme 2. Preparation of **MitoP-3**. *Reagents and conditions* (i) 1,6-diiodohexane, K_2CO_3, MeCN, 100 °C, 3 h; (ii) *p*-nitrobenzyl bromide, K_2CO_3, KI, MeCN, 80 °C, 16 h; (iii) triphenylphosphine, toluene, 105 °C, 16 h.

Photophysical properties

Probes **MitoP-1** and **MitoP-2** and their respective fluorophores **1** and **2** were fully characterized by NMR, UV-Vis and fluorescence spectroscopies.[23] The photophysical properties of these compounds were investigated in three solvent systems: 1,4-dioxane and acetonitrile as examples of low and high polarity organic solvents and a mixture of PBS/DMSO (1/1 v/v, pH = 7.4) as the aqueous environment. The analysis of both absorption and emission spectra clearly evidenced distinct photophysical properties concerning the probes (**MitoP-1** and **MitoP-2**) and their parent fluorophores (**1** and **2**, Figure 4 and 5, Table S1). Regarding the ground state properties, the absorption of both fluorophores **1** and **2,** and probes **MitoP-1** and **MitoP-2,** appeared in the visible range. Fluorophores **1** and **2** disclose similar absorption maxima, perfectly compatible for a selective light excitation using a 405 nm violet-blue diode laser (λ_{abs} = 420 nm, ε ~ 25000 $(M.cm)^{-1}$ for **1**; $\lambda_{abs(PBS/DMSO)}$ = 389 nm, ε ~ 41000 $(M.cm)^{-1}$ for **2**). Concerning the probes, **MitoP-1** and **MitoP-2,** they displayed distinct spectroscopic properties according to one another. As expected, **MitoP-2** features an absorption pattern similar to its parent fluorophore **2** ($\lambda_{abs(PBS/DMSO)}$ = 394 nm, ε ~ 37000 $(M.cm)^{-1}$). However, **MitoP-1** discloses a remarkable redshift and hyperchromic effect in its absorption spectra when compared with **1** ($\lambda_{abs(PBS/DMSO)}$ = 526 nm, ε ~ 54000 $(M.cm)^{-1}$). In fact, the formation of the pyridinium salt substantially strengthen the conjugation, (and the electronic delocalization) between the electron rich *N*,*N*-dimethylaniline moiety and the electron poor pyridinium group, in the ground state, thus generating a bathochromic shift of 106 nm in the absorption maxima of **MitoP-1**. Interestingly, this feature allows a more selective excitation of **1** over **MitoP-1** by using the appropriate excitation wavelength.

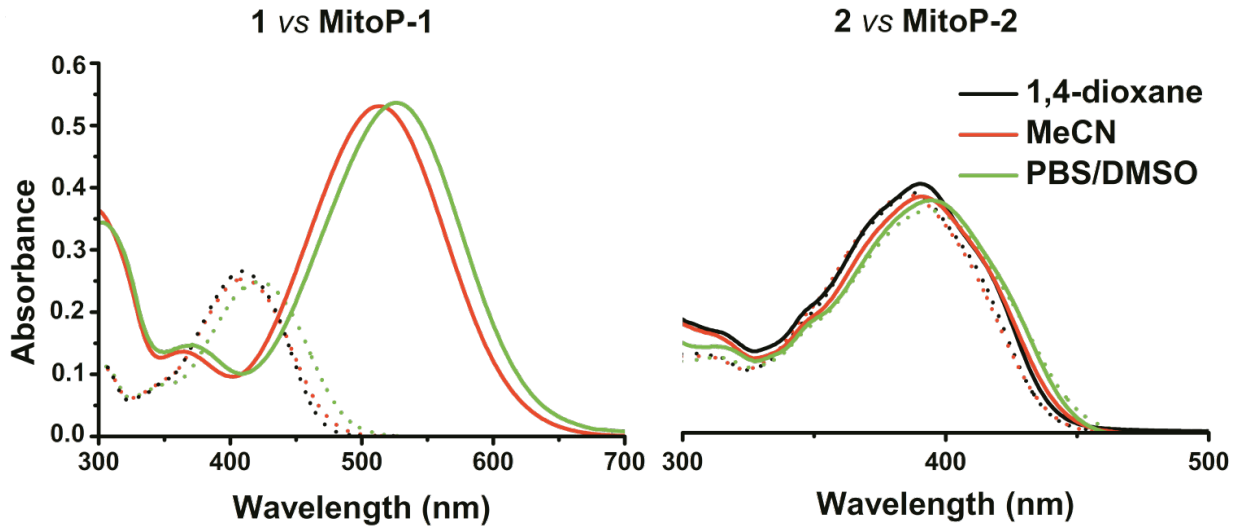

Figure 4. UV-visible absorption spectra of probes **MitoP-1** and **MitoP-2** (bold lines) and their parent fluorophores **1** and **2** (dashed lines) in three different solvents at ~ 10.0 μM (except for **MitoP-1** in 1,4-dioxane because of lack of solubility).

Concerning the fluorescence emission properties, a clear and dramatic drop in the fluorescence intensity was recorded for both probes (ϕ_{fl} < 0.1% for **MitoP-1** and **MitoP-2**, Table S1) when compared with their respective fluorophores **1** and **2** (ϕ_{fl} = 0.17 and 0.50, respectively, in PBS/DMSO mixture). This observation confirms that the attachment of the *p*-nitrobenzyl moiety can trigger the PET mechanisms upon light absorption, thus causing the suppression of the fluorescence emission of these probes. In addition, it is interesting to note that both fluorophores **1** and **2** disclose the gradual bathochromic shift on their emission spectra, with larger Stokes shift values, when ranging from the least to the most polar environment (Figure 5). This observation is consistent with the expected formation of an intramolecular charge transfer (ICT) excited state, as already reported by our group for such group of fluorophores. Altogether, the spectroscopic features of **MitoP-1**, **MitoP-2**, **1** and **2**, strongly support the possibility to use the probes (**MitoP-1**, **MitoP-2**) as reporters of NTRs activity in a fluorescence turn-ON fashion.

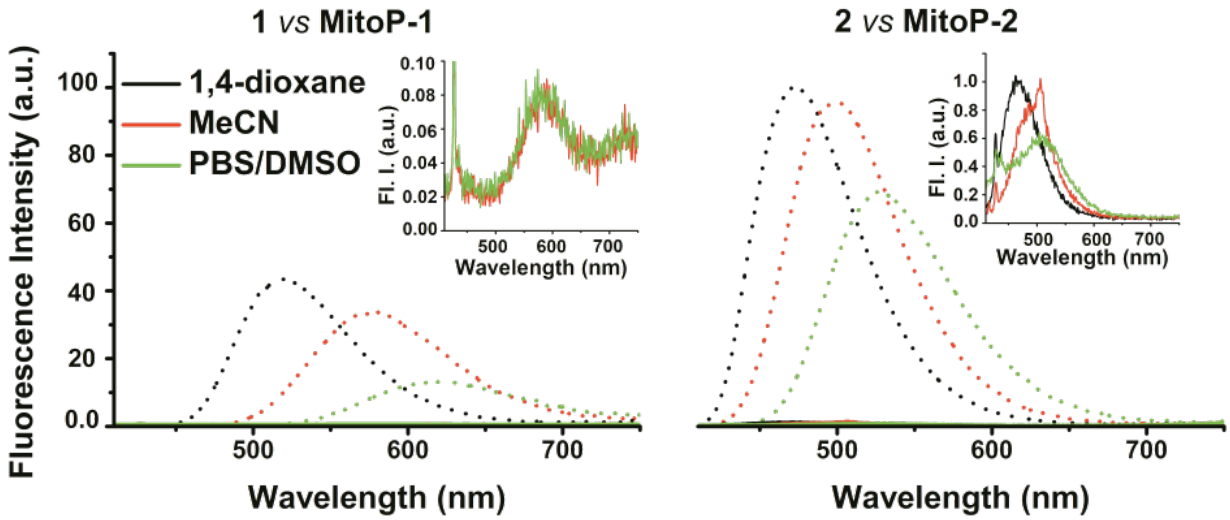

Figure 5. Fluorescence emission spectra of probes **MitoP-1** (λ_{ex} = 405 nm) and **MitoP-2** (λ_{ex} = 405 nm, bold lines) and their parent fluorophores **1** and **2** (dashed lines) in three different solvents at ~ 1.0 μM (except for **MitoP-1** in 1,4-dioxane because of lack of solubility).

Next, we briefly investigated the possible processing of compounds **MitoP-1** and **MitoP-2** by the NTR enzyme and the resulting fluorescence enhancement. For this purpose, we recorded the fluorescence emission spectra of these two probes in simulated physiological conditions (PBS buffer, pH = 7.4) in the absence and after 6 h incubation with *E. coli* NTR (2.5 μg/mL) and NADPH (0.5 mM) as electron donor. As expected, both probes, **MitoP-1** and **MitoP-2**, exhibited very weak fluorescence emissions in the absence of NTR/NADPH.

Surprisingly, in the presence of the enzyme and its cofactor, the expected fluorescence turn-ON signal could only be recorder for **MitoP-2** (Figure 6) and no fluorescence enhancement was observed with **MitoP-1**. These results suggest that **MitoP-1** cannot undergo enzymatic processing of its *p*-nitrobenzyl unit; even after 24 hours of incubation or in the presence of higher concentration of NTR (10 μg/mL, data not shown).

Thus, we focused our first investigations on **MitoP-2**. In fact, in the absence of NTR enzyme, **MitoP-2** probe displays very weak fluorescence emission. Interestingly, after treatment with NTR enzyme (6 h), an important increase in the fluorescence emission intensity was observed (6-fold enhancement). This is consistent with the restauration of the ICT band of fluorophore **2**, triggered by the enzymatic cascade, *i.e.*, processing and cleavage of the *p*-nitrobenzyl moiety originally present on **MitoP-2**. Thereby, these results validate that **MitoP-2** can be further explored for the NTR-sensitive cellular visualization of mitochondria.

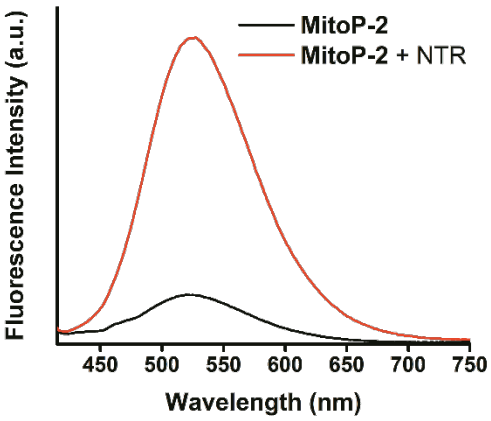

Figure 6. Fluorescence emission spectra of **MitoP-2** in the absence (black line), and after incubation with NTR (2.5 μg/mL, red line) and NADPH (0.5 mM) during 6 h. Conditions: probe concentration ~ 1.0 μM; PBS/DMSO (1/1, v/v, pH = 7.4, 37°C); λ_{ex} = 405 nm.

Before the cellular evaluation of **MitoP-2**, and in view of the lack of enzymatic response of **MitoP-1** to NTR, we decided to complement our study by surveying the third probe, **MitoP-3** which is analogous to **MitoP-2**. As foreseen, it discloses similar photophysical profile (λ_{abs}, λ_{em}, ε and ϕ_{fl}) compared with the parent probe, **MitoP-2** (Table S1, Figure S15). We observed that **MitoP-3** displays very low fluorescent quantum yield values in aqueous and organic media. **MitoP-3** also responded to the processing of its *p*-nitrobenzyl moiety by the NTR, as evidenced by the 11-fold increase in its fluorescence intensity (*vs* 6-fold for **MitoP-2**, for the same incubation time, Figure S16). This observation underlines a smoothly higher sensitivity of **MitoP-3** for the signalling of NTR enzymatic activity *in vitro*.

In cellulo imaging of NTR activity

Following the spectroscopic characterization of probes **MitoP-2** and **MitoP-3**, and the validation to the signalling of a nitroreductase activity *in vitro*, we proceeded to the imaging of the mitochondrial NTR activity using confocal laser scanning microscopy. Two sets of *in cellulo* experiments in A375 melanoma cancer cell line were performed in order to assess: 1- the possible staining of the mitochondria; and 2- the specificity triggered by the selective activation of the probes in response to mitochondrial NTR activity. For these purpose, **MitoP-2** and **MitoP-3** were used in co-localization experiments with Mitotracker Deep Red (MTDR), a commercially available and specific mitochondrial tracker. To our delight, as shown in Figure 7, when A375 cells were successively incubated with our probes and MTDR, they showed the characteristic fluorescence emissions of MTDR (in the red channel) and of **2** or **3** (green channel) with a very high correlation and coverage. It is noteworthy that **MitoP-2** discloses an ability for the specific staining of mitochondria organelles that is comparable to **MitoP-3** without requiring any additional cationic unit for the mitochondrial domains targeting. Moreover, to our knowledge, **MitoP-2**

represents the first neutral profluorescent system reported to visualize mitochondria organelles exploiting the specific mitochondrial NTR activity in cells under normoxic conditions.

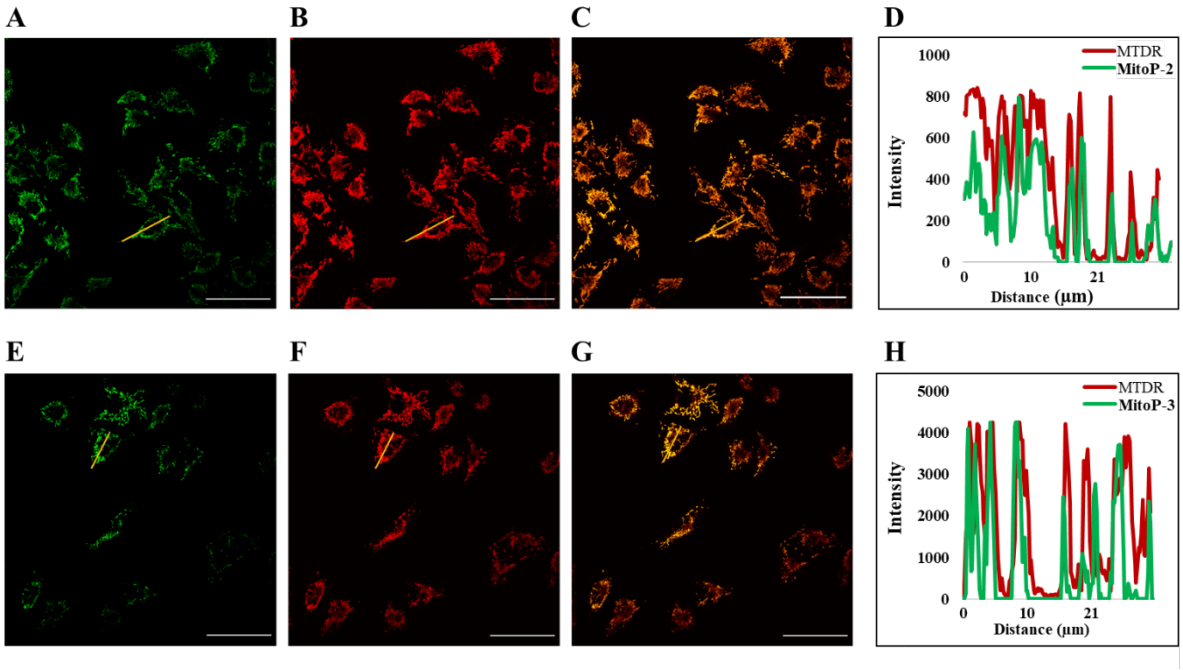

Figure 7. Co-localization experiments of probes **MitoP-2** and MTDR (top line) and **MitoP-3** and MTDR (bottom line), in human melanoma A375 cells. The cells were incubated with **MitoP-2** or **MitoP-3** (0.1 µM) for 30 min at 37°C and the medium was replaced with fresh medium containing MTDR (0.1 µM) and incubated for 30 min. Images for **MitoP-2** (A) and **MitoP-3** (E) and MTDR (B and F) were recorded using excitation wavelengths of 405 and 633 nm, and collection windows were at 500–570 nm and 660–740 nm, respectively. (C and G) Merged images of (A and B) and (E and F). (D and H) Pixel correlation across arrow in (C) and (G). Scale bar: 50 µm.

Having confirmed the selective uptake of both **MitoP-2** and **MitoP-3** by mitochondria, we performed an additional experiment in order to get further insights concerning the enzymatic activation of these probes by the mitochondrial NTRs. For this purpose, we followed the evolution of the fluorescence signal emitted by A375 melanoma cells after different incubation times (5, 15 and 30 minutes, Figure 8) with **MitoP-2** or **MitoP-3**. As expected, a time-dependent increase in the fluorescence emission signal was recorder for both probes; the longer the incubation, the higher the fluorescence response. Altogether, these experiments underpin that both **MitoP-2** and **MitoP-3** have excellent ability to stain mitochondria organelles (regardless of the presence/absence of the cationic mitochondria-targeting unit) with high specificity and very low background emission. The triggering of the fluorescence signal could be *bona fide* imparted to the NTR activity that is specific to the mitochondrion under normoxic conditions.

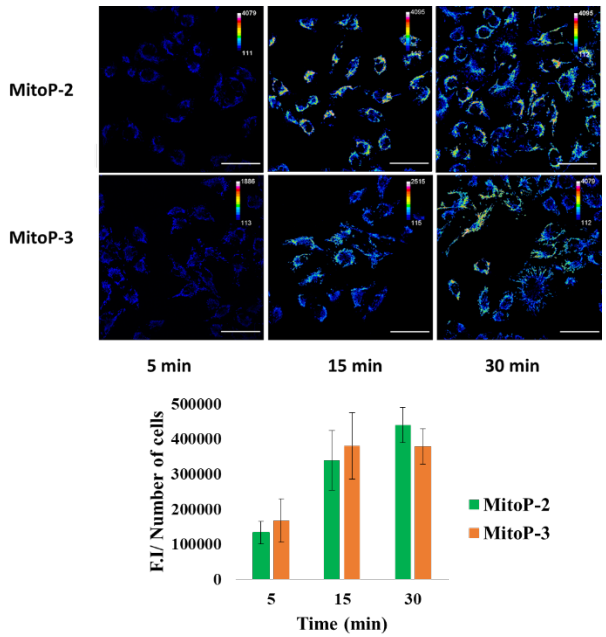

Figure 8. (A) Confocal time-lapse microscopy of human melanoma A375 cells incubated with **MitoP-2** or **MitoP-3** (0.1 µM) during three different times (5, 15 and 30 min). Excitation wavelength of 405 nm and collection window at 500–570 nm, using a Plan Apo 63X oil 1.4 NA objective; scale bars: 50 µm. (B) Quantification of fluorescence intensity of A375 for the different times.

In conclusion, we reported herein the access of two new small molecular probes for the staining mitochondria organelles using a selective mechanism of activation and processing of caged, non-fluorescent precursors by mitochondrial nitroreductase enzymes. Compounds **MitoP-2** and **MitoP-3** proved accessible in only 2 to 3 steps synthetic routes. They were successfully employed as turn-ON fluorescent probes for the detection of the NTR activity in an enzymatic assay. The mechanism associated with the light-up event was attributed to the processing of the *p*-nitrobenzyl unit present on the probes (**MitoP-2** and **MitoP-3**) and the associated release of the parent fluorophore. Beside the enzymatic assay, both probes prove highly efficient in the visualization of mitochondrial NTR activity *in cellulo* under normoxic conditions. Both probes allowed for the specific staining of the mitochondrial compartment as revealed by co-localization experiments performed in the presence of the known MitoTracker Deep Red.

Declaration of Competing Interest

There is no conflict of interest.

Acknowledgemnts

This work was supported by CNRS, University Côte d'Azur, ANR and Cancéropôle PACA.

References

[1] H. Zhu, J. Fan, J. Du, X. Peng, Fluorescent Probes for Sensing and Imaging within Specific Cellular Organelles, Acc. Chem. Res. 49 (2016) 2115–2126. https://doi.org/10.1021/acs.accounts.6b00292.

[2] S.J. Sahl, S.W. Hell, S. Jakobs, Fluorescence nanoscopy in cell biology, Nat. Rev. Mol. Cell Biol. 18 (2017) 685–701. https://doi.org/10.1038/nrm.2017.71.

[3] S.H. Alamudi, Y.T. Chang, Advances in the design of cell-permeable fluorescent probes for applications in live cell imaging, Chem. Commun. 54 (2018) 13641–13653. https://doi.org/10.1039/c8cc08107g.

[4] P. Gao, W. Pan, N. Li, B. Tang, Fluorescent probes for organelle-targeted bioactive species imaging, Chem. Sci. 10 (2019) 6035–6071. https://doi.org/10.1039/c9sc01652j.

[5] H. Chen, D.C. Chan, Mitochondrial Dynamics in Regulating the Unique Phenotypes of Cancer and Stem Cells, Cell Metab. 26 (2017) 39–48. https://doi.org/10.1016/j.cmet.2017.05.016.

[6] J. Nunnari, A. Suomalainen, Mitochondria: In sickness and in health, Cell 148 (2012) 1145–1159. https://doi.org/10.1016/j.cell.2012.02.035.

[7] N.S. Chandel, Evolution of Mitochondria as Signaling Organelles, Cell Metab. 22 (2015) 204–206. https://doi.org/10.1016/j.cmet.2015.05.013.

[8] L.P. Diebold, H.J. Gil, P. Gao, C.A. Martinez, S.E. Weinberg, N.S. Chandel, Mitochondrial complex III is necessary for endothelial cell proliferation during angiogenesis, Nat. Metab. 1 (2019) 158–171. https://doi.org/10.1038/s42255-018-0011-x.

[9] A. Chevalier, Y. Zhang, O.M. Khdour, J.B. Kaye, S.M. Hecht, Mitochondrial Nitroreductase Activity Enables Selective Imaging and Therapeutic Targeting, J. Am. Chem. Soc. 138 (2016) 12009–12012. https://doi.org/10.1021/jacs.6b06229.

[10] W. Qin, C. Xu, Y. Zhao, C. Yu, S. Shen, L. Li, W. Huang, Recent progress in small molecule fluorescent probes for nitroreductase, Chin. Chem. Lett. 29 (2018) 1451–1455. https://doi.org/10.1016/j.cclet.2018.04.007.

[11] S. Samanta, Y. He, A. Sharma, J. Kim, W. Pan, Z. Yang, J. Li, W. Yan, L. Liu, J. Qu, J.S. Kim, Fluorescent Probes for Nanoscopic Imaging of Mitochondria, Chem. 5 (2019) 1697–1726. https://doi.org/10.1016/j.chempr.2019.03.011.

[12] Z. Xu, L. Xu, Fluorescent probes for the selective detection of chemical species inside mitochondria, Chem. Commun. 52 (2016) 1094–1119. https://doi.org/10.1039/c5cc09248e.

[13] Z. Thiel, P. Rivera-Fuentes, Single-Molecule Imaging of Active Mitochondrial Nitroreductases Using a Photo-Crosslinking Fluorescent Sensor, Angew. Chem., Int. Ed. 58 (2019) 11474–11478. https://doi.org/10.1002/anie.201904700.

[14] L. Yang, J.Y. Niu, R. Sun, Y.J. Xu, J.F. Ge, The application of mitochondrial targetable pyronine-pyridinium skeleton in the detection of nitroreductase, Sensors Actuators, B Chem. 259 (2018) 299–306. https://doi.org/10.1016/j.snb.2017.12.011.

[15] S. Luo, R. Zou, J. Wu, M.P. Landry, A Probe for the Detection of Hypoxic Cancer Cells, ACS Sensors. 2 (2017) 1139–1145. https://doi.org/10.1021/acssensors.7b00171.

[16] J. Zhang, H.W. Liu, X.X. Hu, J. Li, L.H. Liang, X.B. Zhang, W. Tan, Efficient Two-Photon Fluorescent Probe for Nitroreductase Detection and Hypoxia Imaging in Tumor Cells and Tissues, Anal. Chem. 87 (2015) 11832–11839. https://doi.org/10.1021/acs.analchem.5b03336.

[17] Z.R. Liu, Y. Tang, A. Xu, W. Lin, A new fluorescent probe with a large turn-on signal for imaging nitroreductase in tumor cells and tissues by two-photon microscopy, Biosens.

Bioelectron. 89 (2017) 853–858. https://doi.org/10.1016/j.bios.2016.09.107.
[18] A.G. Vorobyeva, M. Stanton, A. Godinat, K.B. Lund, G.G. Karateev, K.P. Francis, E. Allen, J.G. Gelovani, E. McCormack, M. Tangney, E.A. Dubikovskaya, Development of a bioluminescent nitroreductase probe for preclinical imaging, PLoS One. 10 (2015) 1–18. https://doi.org/10.1371/journal.pone.0131037.
[19] B. Huang, W. Chen, Y.Q. Kuang, W. Liu, X.J. Liu, L.J. Tang, J.H. Jiang, A novel off-on fluorescent probe for sensitive imaging of mitochondria-specific nitroreductase activity in living tumor cells, Org. Biomol. Chem. 15 (2017) 4383–4389. https://doi.org/10.1039/c7ob00781g.
[20] M. Safir Filho, S. Fiorucci, A.R. Martin, R. Benhida, Design, synthesis and photophysical studies of styryl-based push–pull fluorophores with remarkable solvatofluorochromism, New J. Chem. 41 (2017) 13760–13772. https://doi.org/10.1039/C7NJ03142D.
[21] M. Safir Filho, P. Dao, M. Gesson, A.R. Martin, R. Benhida, Development of highly sensitive fluorescent probes for the detection of β-galactosidase activity – application to the real-time monitoring of senescence in live cells, Analyst. 143 (2018) 2680–2688. https://doi.org/10.1039/C8AN00516H.
[22] M. Safir Filho, P. Dao, A.R. Martin, R. Benhida, Visualization of intracellular lipid droplets using lipophilic benzothiazole-based push-pull fluorophores at ultralow concentration, Dyes Pigm. 167 (2019) 68–76. https://doi.org/10.1016/j.dyepig.2019.04.003.
[23] See ESI for further details.